Selective laser melting produced porous titanium scaffolds regenerate bone in critical size cortical bone defects

J. Van der Stok[1*], O.P. Van der Jagt[1], S. Amin Yavari[2], M.F.P. De Haas[1], J.H. Waarsing[1], H. Jahr[1], E.M.M. Van Lieshout[3], P. Patka[3], J.A.N. Verhaar[1], A.A. Zadpoor[2], H. Weinans[1]

[1] Orthopedic Research Laboratory, Department of Orthopaedics, Erasmus MC, University Medical Center Rotterdam, Rotterdam, the Netherlands

[2] Department of Biomechanical Engineering, Delft University of Technology, Delft, the Netherlands

[3] Department of Surgery-Traumatology, Erasmus MC, University Medical Center Rotterdam, Rotterdam, the Netherlands

*Corresponding author:

Johan van der Stok

Erasmus MC, University Medical Centre

Department of Orthopaedics

Room Ee16-14

P.O. Box 2040

3000 CA Rotterdam

The Netherlands

E-mail: j.vanderstok@erasmusmc.nl

Tel: +31-10-7043384

Fax: +31-10-7044690

Abstract

Porous titanium scaffolds have good mechanical properties that make them an interesting bone substitute material for large bone defects. These scaffolds can be produced with selective laser melting, which has the advantage of tailoring the structure's architecture. Reducing the strut size reduces the stiffness of the structure and may have a positive effect on bone formation. Two scaffolds with struts of 120-micron (titanium-120) or 230-micron (titanium-230) were studied in a load-bearing critical femoral bone defect in rats. The defect was stabilized with an internal plate and treated with titanium-120, titanium-230, or left empty. *In vivo* micro-CT scans at four, eight, and twelve weeks showed more bone in the defects treated with scaffolds. Finally, 18.4±7.1 mm^3 (titanium-120, p=0.015) and 18.7±8.0 mm^3 (titanium-230, p=0.012) bone was formed in those defects, significantly more than in the empty defects (5.8±5.1 mm^3). Bending tests on the excised femurs after twelve weeks showed that the fusion strength reached 62% (titanium-120) and 45% (titanium-230) of the intact contralateral femurs, but there was no significant difference between the two scaffolds. This study showed that in addition to adequate mechanical support, porous titanium scaffolds facilitate bone formation, which results in high mechanical integrity of the treated large bone defects.

Keywords: porous titanium; osteoconduction; bone substitute; bone grafting; micro-CT

1. Introduction

Bone healing requires: 1. cells that are capable of forming bone (osteogenicity), 2. bioactive factors that can attract such cells and initiate bone formation (osteoinduction), 3. a matrix that guides the bone formation (osteoconduction), 4. adequate vascularization and 5. initial mechanical support to the surrounding bone, which becomes more important as the size of the defect increases (1).

Bone defects can be treated with autologous bone. Autologous bone is considered the gold standard treatment and is mostly harvested from the iliac crest. However, the harvesting procedure has a complication rate of 10 to 40%, including hemorrhage, nerve, and vascular lesions and post-operative pain (2). Moreover, the amount and quality of bone that can be harvested is limited, restricting its use

in large defects (3). Therefore, large bone defects are currently treated by distraction osteogenesis, vascularized bone (fibula) grafting, or massive cortical allografts (4). All treatments have their specific disadvantages, such as multiple surgical procedures, high complication rates, and prolonged periods of immobility and rehabilitation.

The challenge is to develop a bone substitute material that enhances bone healing but also offers adequate mechanical strength. Porous titanium scaffolds are especially interesting, since titanium has superior mechanical properties compared to other synthetic materials such as calcium phosphate ceramics and polymers (5). Although the potential of porous titanium has been recognized for many years, development of open porous structures has been hampered by the limitations of available production techniques (6). With production techniques such as plasma spraying (7), space-holder techniques (8), powder metallurgy (9), or sintering of titanium fibers (10) it remains difficult to produce a porous structure with the desired architecture that meets both osteoconductive and mechanical requirements. For osteoconduction, an open interconnected porous structure with pores in the range of 200-500 µm is required (11). From a mechanical point of view, the structure should be stiff enough to sustain the physiological loads, but it should not drastically exceed the stiffness of the bone being replaced to avoid stress shielding.

Better control over the structural architecture can be acquired using selective laser melting (SLM) (12). SLM allows production of very fine and small porous titanium structures, with struts in the range of 100-200 µm. This enables the possibility of tailoring and optimizing the structural and mechanical properties of the scaffolds while maintaining the required pore dimensions that allow for bone and vessel ingrowth. Thinner titanium struts may result in increased elastic and plastic deformation. Such deformation of the porous structure reduces stress-shielding inside the scaffold and may provide a biomechanical stimulus for the bone-forming cells, thereby resulting in more bone formation (13).

In this study, we used a critically sized femoral bone defect in a rat model to test two hypotheses: 1. porous titanium scaffolds can be a biomechanically strong osteoconductive scaffold for repair of

cortical bone defects, 2. thinner strut sizes will result in favorable mechanical properties that will increase bone formation within the titanium scaffold thereby improving mechanical integrity of the treated bone defect.

2. Materials and methods

2.1. Porous titanium scaffolds

Porous titanium scaffolds were produced from Ti6Al4V using SLM (Layerwise, Belgium). Two structural variants were designed using a dodecahedron unit cell as a template structure. One variant consisted of thin titanium struts ('titanium-120') and the second variant consisted of thick titanium struts ('titanium-230'). Both structural variants were produced in two different shapes: 1. cylindrical scaffolds (5 mm Ø x 10 mm) for determining the compression strength and the Young's modulus (supplementary material 1) and 2. femur-shaped scaffolds (6 mm mid-diaphyseal segment of the femur bone, Fig. 1) for determining the ultimate compression force (UCF) (supplementary material 1) and for *in vivo* implantation. All samples underwent post-production chemical and heat treatment to increase surface roughness (supplementary material 2).

2.2. Animal experiment

In 27 male Wistar rats, a 6 mm segmental bone defect of the right femur was created and treated with either titanium-120 (n = 9) or titanium-230 (n = 9) or, was left empty in the control group (n = 9). The local animal ethics committee approved the study. All animals were housed according to the national guidelines for care and use of laboratory animals.

2.2.1 Surgical procedure

A single dose of antibiotics (enrofloxacin, 5 mg/kg body weight) was administered one hour before surgery. The operation was performed aseptically under general anesthesia (1-3.5% isoflurane). The right femur was exposed though a lateral incision of the skin and division of the underlying fascia. A 23 mm long PEEK plate (RatFix, AO Foundation, Switzerland) was fixated to the anterolateral plane of the femur. Three proximal and three distal screws fixated the plate. The periostium was removed

over approximately 8 mm of the mid-diaphysial region before removal of the 6 mm long bone segment. The bone segment was removed with a tailor-made saw guide and a wire saw (RatFix, AO Foundation, Switzerland), and the scaffold was placed press-fit into the defect site. The fascia and skin were sutured in layers and prophylactic pain medication (buprenorphine, 0.05 mg/kg body weight) was administered twice a day for the first three days after surgery. Fluorescent dyes were administered at four (tetracyclin, 25 mg/kg body weight), eight (calcein, 25 mg/kg body weight), and eleven weeks (xylenol orange, 90 mg/kg body weight).

2.2.2. Micro-CT evaluation

Immediately after the surgery, while the rats were still under general anesthesia, a SkyScan 1076 scanner (Bruker micro-CT, Belgium) was used in order to acquire a baseline *in vivo* micro-CT scan. A 36 µm-resolution protocol was used at 95 kV, 1.0 mm Al filter, and 0.6 degree rotation step, resulting in a 15 minute scan. *In vivo* scans were repeated after four, eight, and twelve weeks. For the final *ex vivo* scan, an 18 µm-resolution protocol was used at 95 kV, 1.0 mm Al/0.25 mm Cu filter, and 0.4 degree rotation step (3 h scan). The CT images were reconstructed using volumetric reconstruction software NRecon version 1.5 (Bruker micro-CT, Belgium).

The total bone volume (TBV) was defined as the total bone volume within the 6 mm defect segment including bone formed around the titanium scaffold (Fig. 2A) The bone volume in pores (BVp) was defined as the bone volume measured within the pore volume (PV) of the titanium scaffold (Fig. 2B), and is also expressed as a percentage of the pore volume (BVp/PV). TBV and BVp were determined using software CTAnalyser version 1.11 (Bruker micro-CT, Belgium) (supplementary material 3).

2.2.3. Biomechanical evaluation

The final strength of the treated femurs was measured with three-point bending tests conducted on five samples from each group. In these tests, both supports are chosen as close as possible to the bone-scaffold interfaces (distance < 5 mm). Small distance between the bone-scaffold interfaces and the supports ensures that the three-point bending test measures the interface strength of bone and scaffold

as closely as possible. The contralateral femurs served as controls. To ensure that we tested the entire spectrum, we first sorted the treated femurs according to their BVp and then included every other femur. The bending tests were carried out using a Zwick test machine (Zwick GmbH, Germany) as follows: first, the PEEK plate was carefully removed; the femurs were then supported at the proximal and distal side using two plates that were secured with screws. A plate that exceeded the average pore size applied a downward force to the middle of the porous titanium scaffold, pushing it outside the bone defect. The bending tests were performed at a displacement rate of 2 mm/min until the peak load was reached. The force-displacement curves were recorded and used to determine the maximum force.

2.2.4. Histological evaluation

Histology was performed on four femurs of each group to study the bone-titanium interface and bone morphology. The specimens were dehydrated in a graded ethanol series, and embedded in methylmethacrylate. Sections of ~20 µm were obtained using a diamond saw (Leica SP1600) and stained with basic fuchsin 0.3% solution (Sigma) and methylene blue 1% solution (Sigma). Bone stains red with basic fuchsin and fibrous tissue stains blue with methylene blue. Unstained sections were examined using an epifluorescent microscope (Axiovert 200MOT/Carl Zeiss) with a triple filter block.

2.3. Statistics

Statistical analyses were performed using SPSS Statistics 17.0 (SPSS Inc, Chicago, Ill). The data are presented as means with standard deviation. One-way Analysis of Variation (ANOVA) and subsequent post-hoc pairwise comparisons with Bonferroni adjustment was used to analyze the differences between the three groups. A repeated measures general linear model was used when examining the longitudinal *in vivo* micro-CT data. A Pearsons correlation coefficient was used to determine the correlation between BVp, TBV, and the maximum bending force.

3. Results

3.1. Porous titanium scaffolds

The different titanium strut sizes and equal pore dimensions resulted in a porosity of 88% in the titanium-120 scaffolds and 68% in the titanium-230 scaffolds (Table 1). The titanium-120 structure had five-fold lower compression strength and a four-fold lower homogenized Young's modulus than the titanium-230 structure (Table 1). There was a significant difference in the UCF ($p<0.001$). The UCF of the titanium-230 scaffolds (530±85 N) was higher than the corresponding bone segments (441±31 N, $p=0.022$), whereas the UCF of titanium-120 scaffolds (84±11 N) was lower than the corresponding bone segments ($p<0.001$) (Fig. 3).

3.2. Micro-CT evaluation

Correct positioning of the porous titanium scaffolds was confirmed by micro-CT directly after surgery in all animals and no dislocation of the porous titanium scaffolds was detected during the follow-up. The titanium-230 structure remained completely intact in all rats, whereas breakage of some struts was seen in six of the nine rats given titanium-120. This occurred after either four (two cases) or eight weeks (four cases), but did not result in loss of fixation or complete loss of structural integrity of the scaffolds. The porous titanium scaffolds were well integrated with the adjacent cortical bone and a progression of the bony bridging was observed over time (Fig. S1), although in some rats small areas of the adjacent cortical underwent changes that may indicate bone resorption (Fig. S2). In the empty control group, loss of fixation, due to breakage of the screws, occurred in six out of nine rats. This happened to one rat at four weeks, to four rats at eight weeks, and to one rat at twelve weeks. Those rats were taken out of the experiment at subsequent time points. In the remaining rats, no bridging of the defect had occurred and a consistent pattern of bone resorption of the remaining cortical bone was observed (Fig. S3).

Treatment with porous titanium scaffolds resulted in more TBV than in the empty controls at all time points (Fig. 4A). The increase of TBV was most profound between four and twelve weeks, whereas in the empty controls TBV seemed to have reached a plateau phase after eight weeks. At

twelve weeks, a significant difference in the TBV (p=0.008) was found (Fig 4B). The TBV of the titanium-120 group (18.4±7.1 mm^3) and the titanium-230 group (18.7±8.0 mm^3) was significantly higher than in TBV of the empty control group (5.8±5.1 mm^3, p=0.015 and p=0.012 respectively).

The porous structure of the titanium scaffolds facilitated bone ingrowth given that an increase of BVp was found at all time points (Fig 5A). At twelve weeks, the absolute BVp was 7.4±2.3 mm^3 in the titanium-120 scaffolds and 6.0±2.7 mm^3 in the titanium-230 scaffolds (p=0.38) (Fig. 5B). This resulted in a BVp/PV of 16±5 % in the titanium-120 and 20±9 % in the titanium-230.

3.3. Biomechanical evaluation

The intact femurs that served as control broke at a force of 233±27N. The bending force of the titanium-120-treated femurs was 144±73N (62% of control) compared with 104±38N (45% of control) for titanium-230-treated femurs (Fig. 6A). Except for one case, all samples broke at the titanium-bone interface. BVp measured with micro-CT strongly correlated with the maximum bending force for the titanium-120 group (r^2=0.83, p=0.03). The two treated femurs in which more than 8 mm^3 bone had formed within the pores had a bending force comparable with the intact control femurs (Fig. 6B). For the titanium-230 group, the maximum bending force did not seem to relate to BVp (r^2=0.02, p=0.84).

3.4. Histological evaluation

In the histological evaluation, the empty defect sites showed limited bone formation and resorption of the cortical bone at the proximal and distal sites (Fig. 7A and F). Within the remaining defect area, abundant fibrous tissue was found.

Histology of the titanium groups revealed formation of a major plug of new bone in the medullary canal at both ends of the bone defect. This bone is most likely formed through the process of direct ossification (Fig. 7B and D). The newly formed bone extents from this plug into the porous titanium and the inner space of the scaffold. Bone was also abundant at the outer area of the scaffolds, showing signs of an attempt to bridge the defect area. The area inside the porous titanium that was not

filled with bone was filled with fibrous tissue. The pattern observed correlated well with the bone seen on the corresponding micro-CT images (Fig. 7G and H).

Bone is directly formed on the surface of the porous titanium scaffold. At some areas, however, a thin layer of fibrous tissue between the titanium and the bone was observed (Fig. 7E). No signs of foreign body reactions or inflammation were detected. In one titanium-120 sample, a possible development of a hypertrophic non-union was seen, since a cluster of chondrocytes was found at a site suspect to breakage of titanium struts (Fig. 7C).

The injected fluorochrome labels showed the mineralized bone at four (red), eight (green) and twelve weeks (yellow) (Fig. 8). The observed pattern of fluorochrome labels indicate that bone formation was most active around the titanium-bone interface at the proximal and distal ends of the porous titanium scaffolds (Fig. 8D). Only limited progression of the bridging of the bone defect through the medullary cannel was seen between the four and twelve weeks (Fig. 8C), since the label injected at four weeks (red) was found close to the most advanced bone fronts (yellow).

4. Discussion

This longitudinal *in vivo* study supports our first hypothesis that porous titanium scaffolds provide mechanical support in the early phase after implantation, and facilitate bone formation (osteoconduction) over time, resulting in good mechanical strength of the treated femurs after twelve weeks. A lower titanium strut size reduced the homogenized Young's modulus of the scaffold but did not result in significantly more bone formation or higher mechanical strength of the treated femurs, meaning that these experiments did not support our second hypothesis.

The osteoconductive properties of porous titanium scaffolds were proven by the fact that more bone had formed in the bone defects treated than in the defects that were left empty. This is in line with previous reports that used a metaphyseal bone defect model in rabbits (14; 21-24). The rat femur bone defect model used here has the advantage that it allows for in vivo micro-CT scanning to monitor bone formation throughout time. Bone formation was measured using a custom-made algorithm that

first removed the metal artifacts and then selected the areas of newly formed bone (supplementary material 3). Accurate selection of bone was verified using the corresponding histological sections as a reference (Fig. 7). The *in vivo* bone measurements showed a gradual increase in bone formation in the rats that received titanium-120 or titanium-230 scaffolds, this bone formation may have still been ongoing, because no plateau phase was reached within the twelve weeks follow-up period (Fig 4A).

The increase in bone regeneration seen in the defects treated with porous titanium scaffolds may be related to the scaffold structure and its mechanical properties. The structure of osteoconductive scaffolds is well defined in terms of pore size, interconnectivity, and porosity (11) and these criteria were met for both structural variants. However, the mechanical properties of the two structural variants were different due to their different strut sizes. Reducing the strut size by ~50% in the titanium-120 structure resulted in a large decrease of the homogenized Young's modulus (Table 1). The measured homogenized Young's modulus for the titanium-120 is close to the lowest range reported in the literature for porous titanium (8; 14-17) and within the range of human trabecular bone (0.01-2 GPa) (18). Such low homogenized Young's modulus allows for more deformation upon loading, and was therefore hypothesized to result in more bone ingrowth in the titanium-120 scaffolds. However, there was not significantly more bone formed after twelve weeks (Fig 5B) and a possible explanation could be that the loads that were applied to the titanium-120 scaffolds after implantation in the femoral bone defect were not able to reach the minimum force required to deform the scaffolds.

Defining the mechanical properties that would have allowed deformation of the porous titanium scaffolds after implantation was complicated by a number of factors. Although the titanium-120 was significantly weaker than the femur segment that it replaced and the titanium-230 was significantly stronger in term of UCF, however bone is able to withstand forces that are at least twice the normal peak loading (19). Furthermore, different bones and even different areas of a bone can have different mechanical properties (18). Finally, not all the mechanical loads will be transferred through the porous titanium scaffolds, since a portion of the load will be transferred to the PEEK

fixation plate. Preliminary results of a finite element model of this femur bone defect indicates that the division of force is highly dependent on the stiffness of the scaffold, the contact conditions between the scaffold and bone, and the mechanical loading (20). Moreover, the load distribution changes over time as more bone is generated within the scaffold. Taking into account all these factors to define the optimal mechanical properties of porous titanium scaffolds remains difficult. One should therefore take the species, the type of bone that needs to be replaced, and the applied fixation methods into account.

Implantation of the titanium scaffolds provided sufficient support to the bone defect, because it did not result in a loss of fixation, whereas in most rats for which the defect was left empty the PEEK plate fixation failed. The ability to provide sufficient support is likely to have contributed to the bone formation in the defect area but is only made possible by the mechanical properties that allow the porous titanium scaffold to function as a load-bearing scaffold in this rat femur defect. The final strength of the treated femurs was measured using three-point bending test. In the three-point bending test, the supports were chosen very close to the bone-scaffold interface, so that the bending test more or less measures the interface strength between bones and scaffold and is therefore somewhat similar to torsion test. The bending forces are surprisingly high, taking into account twelve weeks implantation period and that only about 20% of the pore volume was occupied by newly formed bone. The broken struts seen in the titanium-120 scaffolds, which itself could be explained by the limited compression strength, did not have a negative impact on the maximum bending force. In fact, the maximum bending force was even somewhat higher in the titanium-120 group compared to the titanium-230 group (Fig 6A). Interestingly, there is a strong correlation between the bending force and the bone volume inside the pores for the titanium-120 scaffolds but not for titanium-230. Possible factors other than bone volume that may affect the strength of the treated femurs could be the bone-titanium bonding. Previous studies that used similar heat and surface treatments showed good bone-bonding and even indicated a possible osteoinductive role of the modified surface (25). The larger

surface area in the titanium-120 scaffolds (Table 1) may have resulted in a larger area of direct bone-titanium contact. This may explain why bone volume within the pores shows a better correlation with the final mechanical strength for the femurs that received a titanium-120 scaffold than those that received titanium-230.

The work presented here shows the potential of porous titanium scaffolds, and especially the possibility to function as a load-bearing scaffold may become relevant in clinical cases where conventional fixation methods alone may be insufficient. But before porous titanium can be used in clinical cases, the mechanical properties should be tailored to the human situation. Another aspect of porous titanium that should be further explored is the surface. Surface modifications have been studied by others (26), and it presents a great opportunity to enhance bone-titanium bonding or increase bone formation. A possible example would be the addition of a calcium phosphate coating (27). The surface may also be used to address the main drawback of titanium implants, *i.e.* the risk of infection. Antibiotic coatings have already been developed for solid implants (28), and they may help to reduce the risk of infection. The challenge will be to combine all these different techniques into one porous titanium scaffold that can withstand thorough experimental testing before proceeding to clinical trials.

5. Acknowledgements

This research forms part of the Project **P2.04 BONE-IP** of the research program of the **BioMedical Materials** institute, co-funded by the **Dutch Ministry of Economic Affairs, Agriculture and Innovation**.

References

1. Giannoudis, P.V., Einhorn, T.A., Marsh, D. 2007. Fracture healing: the diamond concept. Injury 38 Suppl 4: S3-6.

2. Younger, E.M., Chapman, M.W. 1989. Morbidity at bone graft donor sites. J Orthop Trauma 3: 192-195.

300 3. Damien, C.J., Parsons, J.R. 1991. Bone graft and bone graft substitutes: a review of current
301 technology and applications. J Appl Biomater 2: 187-208.
302 4. Pneumaticos, S.G., Triantafyllopoulos, G.K., Basdra, E.K., Papavassiliou, A.G. 2010. Segmental
303 bone defects: from cellular and molecular pathways to the development of novel biological treatments.
304 J Cell Mol Med 14: 2561-2569.
305 5. Van der Stok, J., Van Lieshout, E.M., El-Massoudi, Y., Van Kralingen, G.H., Patka, P. 2011. Bone
306 substitutes in the Netherlands - a systematic literature review. Acta Biomater 7: 739-750.
307 6. Murr, L.E., Gaytan, S.M., Medina, F., Lopez, H., Martinez, E., Machado, B.I., Hernandez, D.H.,
308 Martinez, L., Lopez, M.I., Wicker, R.B., Bracke, J. 2010. Next-generation biomedical implants using
309 additive manufacturing of complex, cellular and functional mesh arrays. Philos Transact A Math Phys
310 Eng Sci 368: 1999-2032.
311 7. Fujibayashi, S., Neo, M., Kim, H.M., Kokubo, T., Nakamura, T. 2004. Osteoinduction of porous
312 bioactive titanium metal. Biomaterials 25: 443-450.
313 8. Singh, R., Lee, P.D., Lindley, T.C., Kohlhauser, C., Hellmich, C., Bram, M., Imwinkelried, T.,
314 Dashwood, R.J. 2010. Characterization of the deformation behavior of intermediate porosity
315 interconnected Ti foams using micro-computed tomography and direct finite element modeling. Acta
316 Biomater 6: 2342-2351.
317 9. Dabrowski, B., Swieszkowski, W., Godlinski, D., Kurzydlowski, K.J. 2010. Highly porous titanium
318 scaffolds for orthopaedic applications. J Biomed Mater Res B Appl Biomater 95: 53-61.
319 10. Vehof, J.W., Spauwen, P.H., Jansen, J.A. 2000. Bone formation in calcium-phosphate-coated
320 titanium mesh. Biomaterials 21: 2003-2009.
321 11. Daculsi, G., Passuti, N. 1990. Effect of the macroporosity for osseous substitution of calcium
322 phosphate ceramics. Biomaterials 11: 86-87.

12. Hollander, D.A., von Walter, M., Wirtz, T., Sellei, R., Schmidt-Rohlfing, B., Paar, O., Erli, H.J. 2006. Structural, mechanical and in vitro characterization of individually structured Ti-6Al-4V produced by direct laser forming. Biomaterials 27: 955-963.

13. Spoerke, E.D., Murray, N.G., Li, H., Brinson, L.C., Dunand, D.C., Stupp, S.I. 2008. Titanium with aligned, elongated pores for orthopedic tissue engineering applications. J Biomed Mater Res A 84: 402-412.

14. Bandyopadhyay, A., Krishna, B.V., Xue, W., Bose, S. 2009. Application of laser engineered net shaping (LENS) to manufacture porous and functionally graded structures for load bearing implants. J Mater Sci Mater Med 20 Suppl 1: S29-34.

15. Heinl, P., Muller, L., Korner, C., Singer, R.F., Muller, F.A. 2008. Cellular Ti-6Al-4V structures with interconnected macro porosity for bone implants fabricated by selective electron beam melting. Acta Biomater 4: 1536-1544.

16. Ryan, G., McGarry, P., Pandit, A., Apatsidis, D. 2009. Analysis of the mechanical behavior of a titanium scaffold with a repeating unit-cell substructure. J Biomed Mater Res B Appl Biomater 90: 894-906.

17. Xue, W., Krishna, B.V., Bandyopadhyay, A., Bose, S. 2007. Processing and biocompatibility evaluation of laser processed porous titanium. Acta Biomater 3: 1007-1018.

18. An, Y.N. 1999. Mechanical properties of bone. In: An, Y.N., Draughn, R.A. (Eds.), Mechanical testing of bone and the bone-implant interface. CRC Press: New York, pp. 41-63.

19. Biewener, A.A. 1993. Safety factors in bone strength. Calcif Tissue Int 53 Suppl 1: S68-74.

20. Poelert, S., Campoli, G., Van der Stok, J., Amin Yavari, S., Weinans, H., Zadpoor, A.A. 2012. Relating the microstructure of titanium foam to load distribution and induced bone ingrowth. In, ESB2012. Lisbon.

21. Faria, P.E., Carvalho, A.L., Felipucci, D.N., Wen, C., Sennerby, L., Salata, L.A. 2010. Bone formation following implantation of titanium sponge rods into humeral osteotomies in dogs: a histological and histometrical study. Clin Implant Dent Relat Res 12: 72-79.

22. Lopez-Heredia, M.A., Goyenvalle, E., Aguado, E., Pilet, P., Leroux, C., Dorget, M., Weiss, P., Layrolle, P. 2008. Bone growth in rapid prototyped porous titanium implants. J Biomed Mater Res A 85: 664-673.

23. Pattanayak, D.K., Fukuda, A., Matsushita, T., Takemoto, M., Fujibayashi, S., Sasaki, K., Nishida, N., Nakamura, T., Kokubo, T. 2011. Bioactive Ti metal analogous to human cancellous bone: Fabrication by selective laser melting and chemical treatments. Acta Biomater 7: 1398-1406.

24. Willie, B.M., Yang, X., Kelly, N.H., Merkow, J., Gagne, S., Ware, R., Wright, T.M., Bostrom, M.P. 2011. Osseointegration into a novel titanium foam implant in the distal femur of a rabbit. J Biomed Mater Res B Appl Biomater 92: 479-488.

25. Takemoto, M., Fujibayashi, S., Neo, M., Suzuki, J., Matsushita, T., Kokubo, T., Nakamura, T. 2006. Osteoinductive porous titanium implants: effect of sodium removal by dilute HCl treatment. Biomaterials 27: 2682-2691.

26. Wennerberg, A., Albrektsson, T. 2009. Effects of titanium surface topography on bone integration: a systematic review. Clin Oral Implants Res 20 Suppl 4: 172-184.

27. Narayanan, R., Seshadri, S.K., Kwon, T.Y., Kim, K.H. 2008. Calcium phosphate-based coatings on titanium and its alloys. J Biomed Mater Res B Appl Biomater 85: 279-299.

28. Zhao, L., Wang, H., Huo, K., Cui, L., Zhang, W., Ni, H., Zhang, Y., Wu, Z., Chu, P.K. 2011. Antibacterial nano-structured titania coating incorporated with silver nanoparticles. Biomaterials 32: 5706-5716.

29. Cory, E., Nazarian, A., Entezari, V., Vartanians, V., Muller, R., Snyder, B.D. Compressive axial mechanical properties of rat bone as functions of bone volume fraction, apparent density and micro-ct based mineral density. J Biomech 43: 953-960.

372 **Tables**

373 **Table 1: Structural and mechanical characteristics of porous titanium scaffolds**

374

	Titanium-120	Titanium-230	Cortical bone (rat)
Porosity (%)	88	68	
Titanium thickness (μm)	120	230	
Pore size (μm)	490 (240-730)	490 (240-730)	
Surface area / volume (μm^2)	0.034	0.018	
Compression strength (MPa)	14.3±1.7	77.7±12.8	140±19 (29)
Homogenized Young's modulus (GPa)	0.38±0.04	1.56±0.21	8.80±2.53 (29)

375 Pore size is presented as median and range. Compression strength and homogenized Young's

376 modulus is presented as average + SD.

377

Figure legends

Figure 1: Femur-shaped porous titanium scaffolds

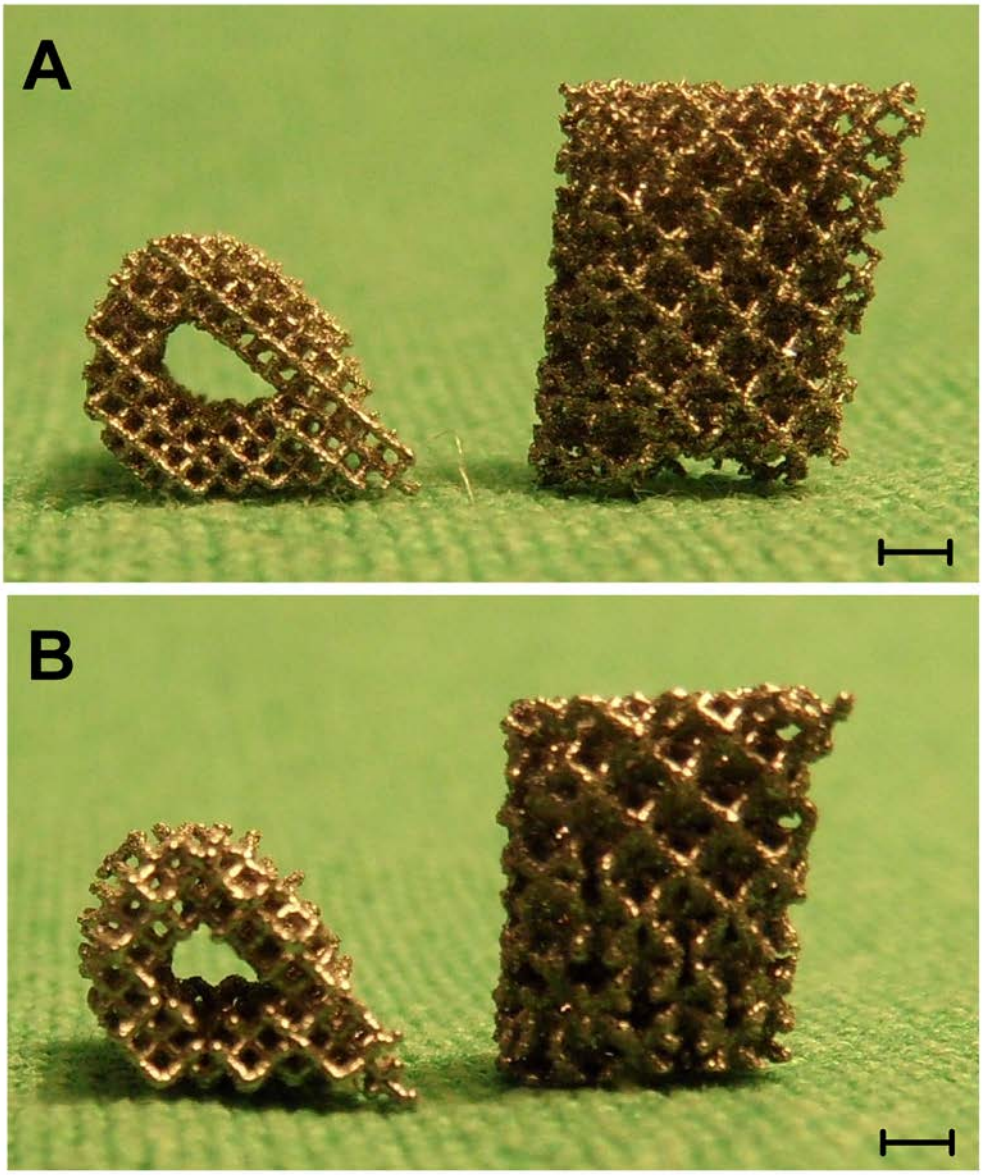

Titanium-120 structure (A) and titanium-230 structure (B). Bar indicates 1 mm.

Figure 2: CT measurements

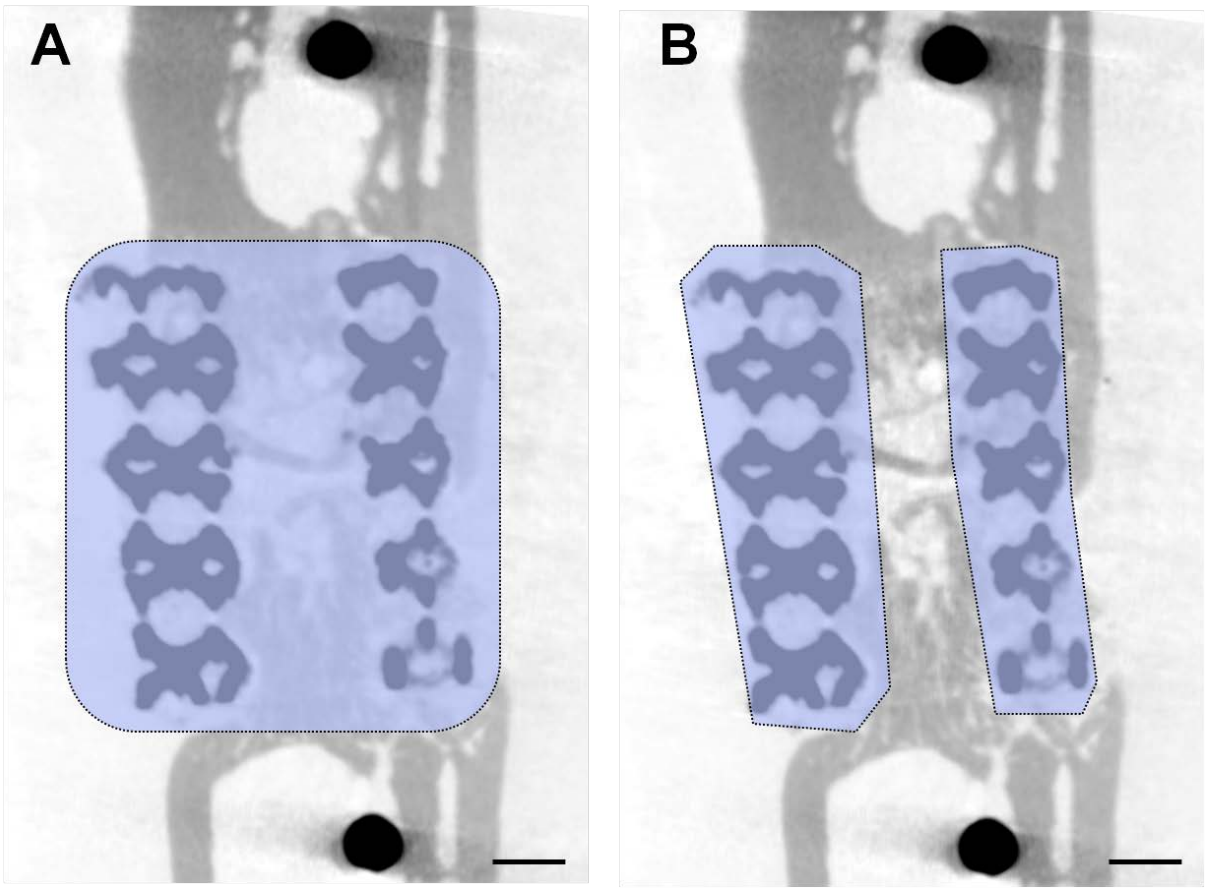

Transversal micro-CT image with volume of interest (blue) used for measurements of TBV (A) and BVp (B). Bar indicates 1 mm.

388 **Figure 3: Ultimate compression force of titanium-120, titanium-230, and cortical bone**

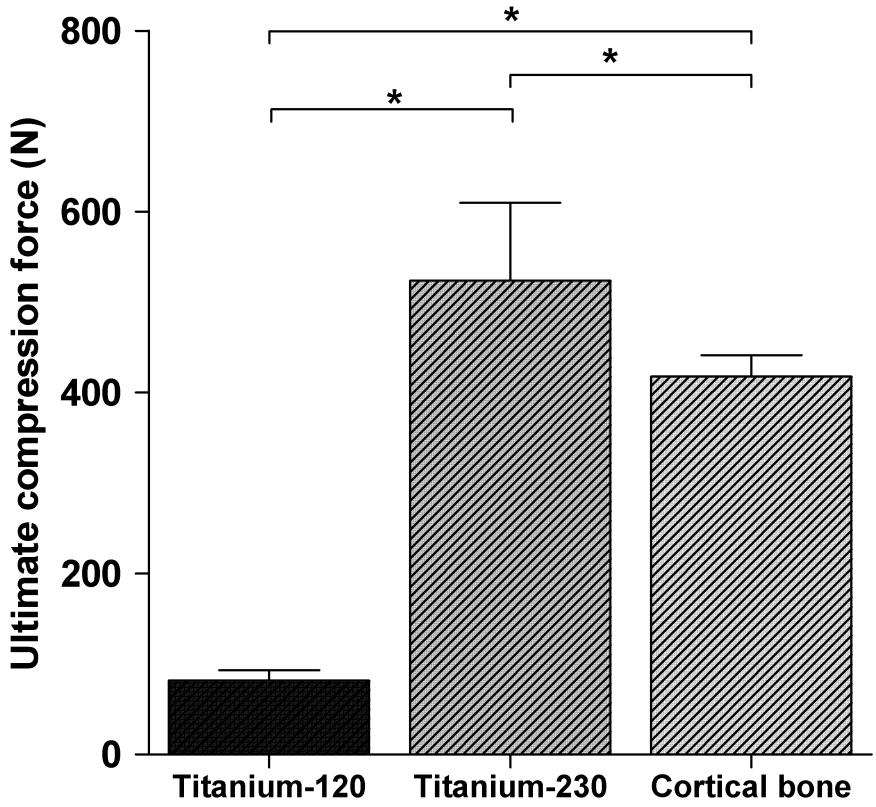

389

390 Statistical analysis was performed with One-Way analysis of Variance (ANOVA) subsequent post-

391 hoc pairwise with Bonferroni adjustment, * is $p<0.05$.

392

Figure 4: Total bone volume

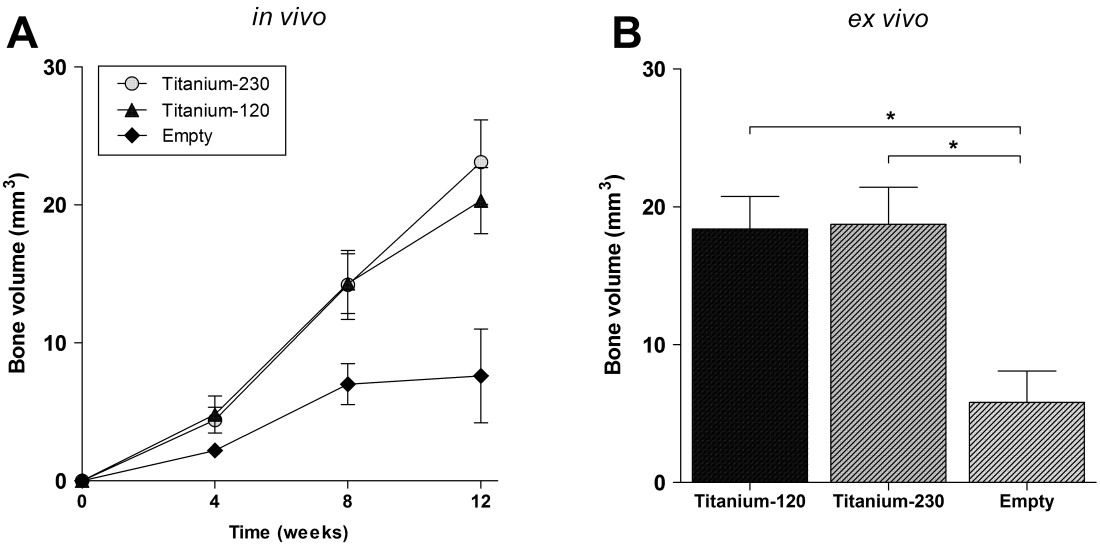

Total bone volume (TBV) measured *in vivo* during the study period (A) and *ex vivo* at twelve weeks (B). The *in vivo* measurements were corrected for artifacts using the scan made at time point zero. Statistical analysis was performed with One-Way analysis of Variance (ANOVA) subsequent post-hoc pairwise with Bonferroni adjustment, * is $p<0.05$.

Figure 5: Bone volume in pores

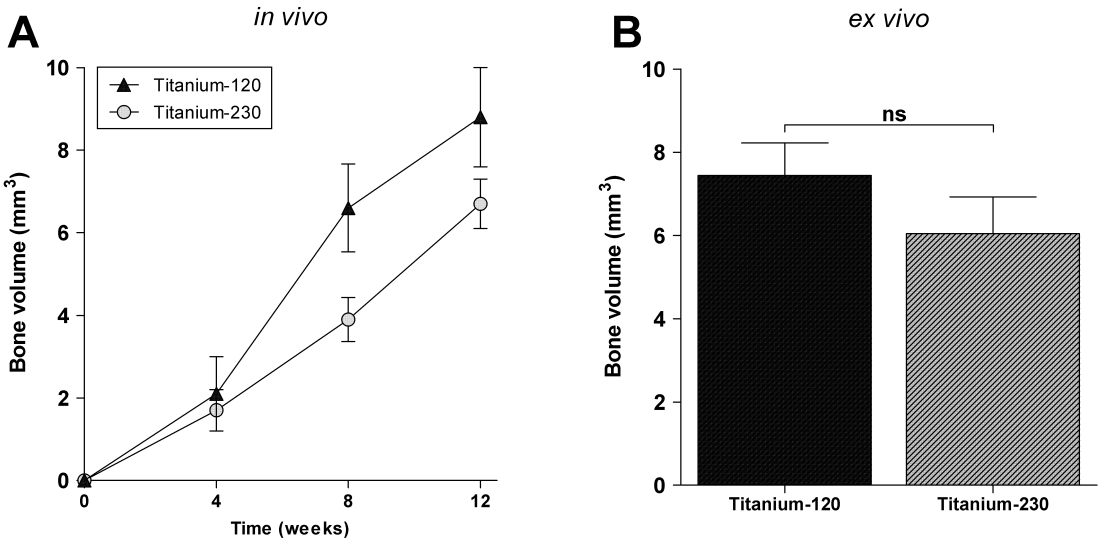

Bone volume in pores (BVp) measured *in vivo* during the study period (A) and *ex vivo* at twelve weeks (B). The *in vivo* measurements were corrected for artifacts using the scan made at time point zero. Statistical analysis was performed with One-Way analysis of Variance (ANOVA), NS is not statistically significant.

Figure 6: Biomechanical bending test

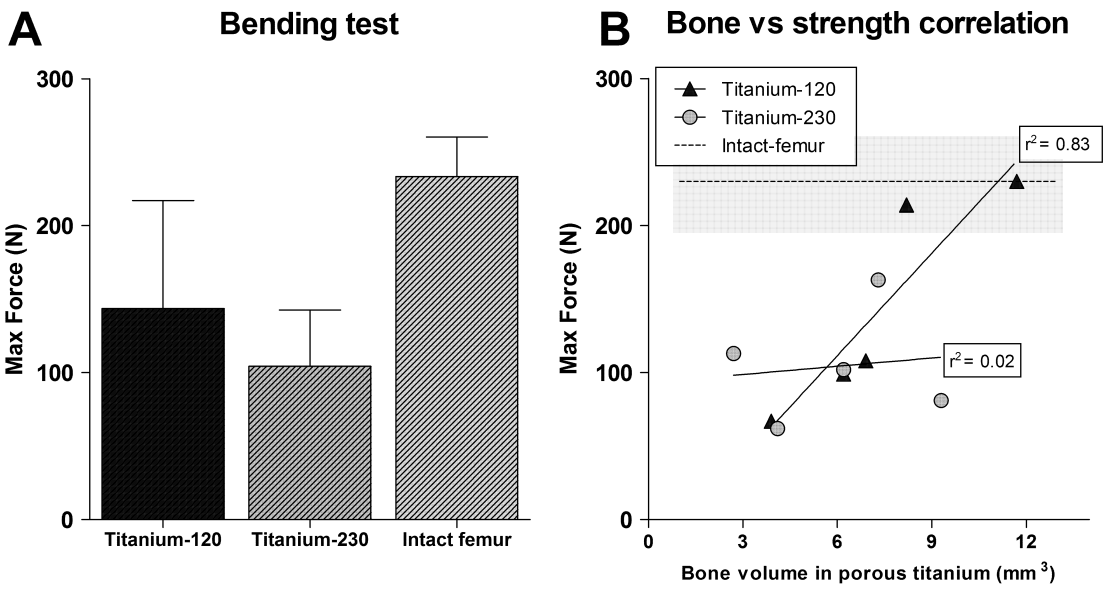

Average maximum bending force (A) and bending force correlated to bone in pore volume (B).

411 **Figure 7: Histology and micro-CT**

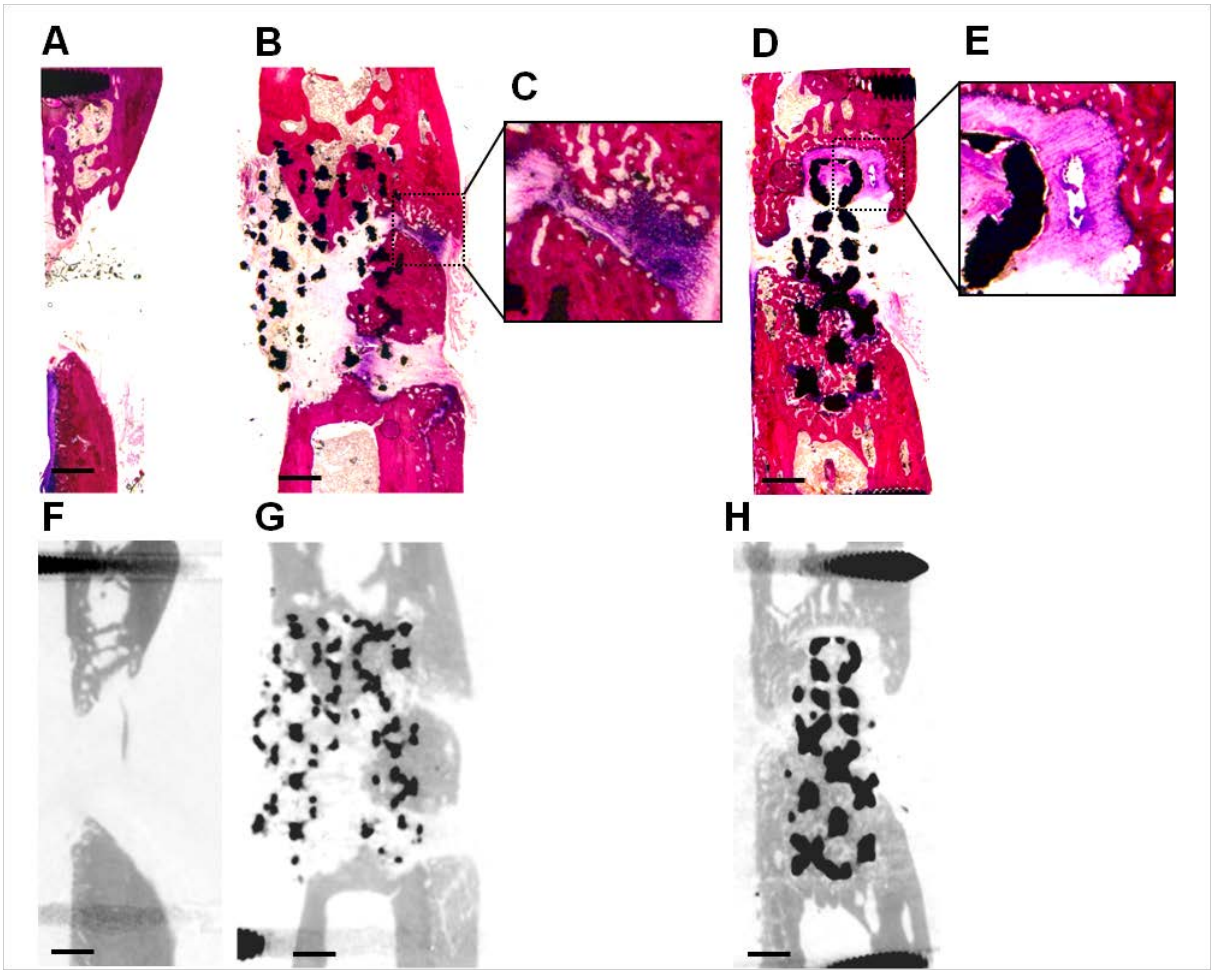

412

413 Histological slides with corresponding micro-CT images of an empty defect (A and F), titanium-120

414 (B and G) and titanium-230 (D and H), including detailed interface view for titanium-120 (C) and

415 titanium-230 (E). Black bar indicates 1 mm.

416

Figure 8: Fluorochrome labeling

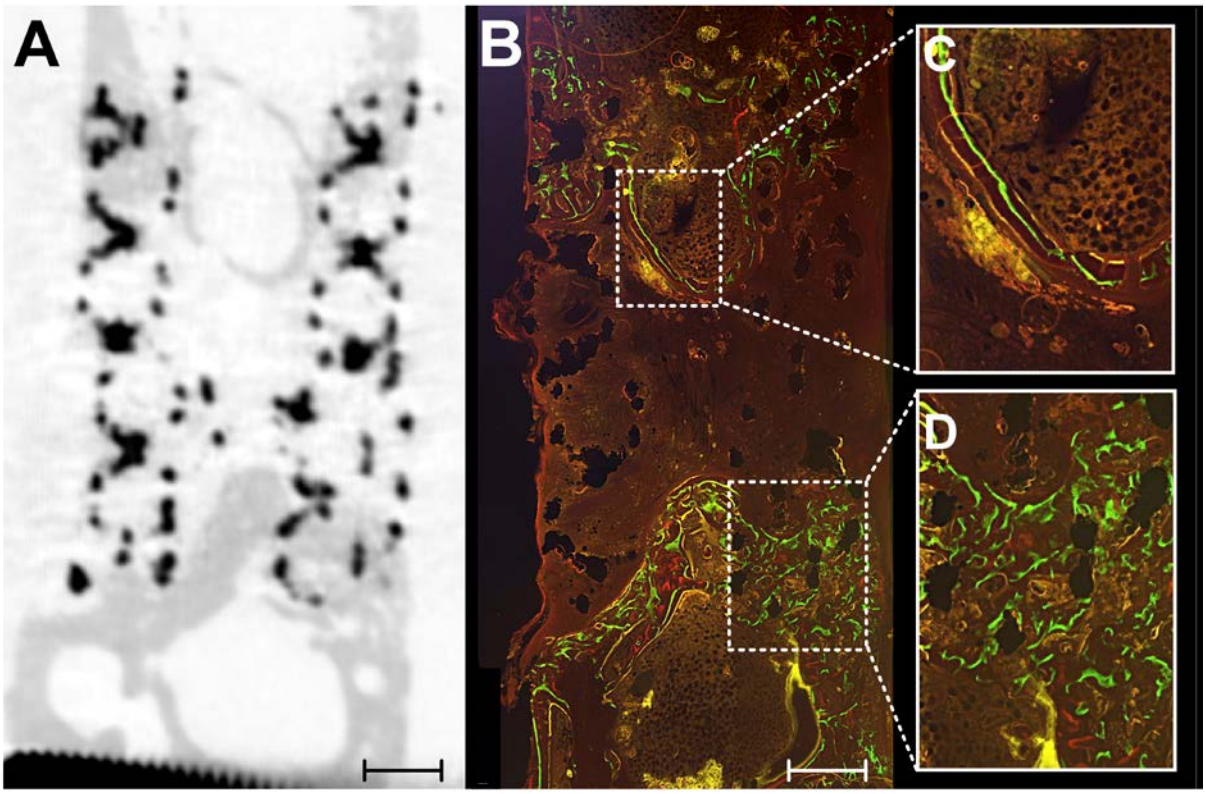

Light microscopy images of the fluorochrome labels of a femur treated with titanium-120 (A) including corresponding histological (B) and micro-CT (C) images. The asterisks indicate active mineralization at the titanium-bone interface, white arrows indicate limited activity at the bone fronts in the medullary canal. Tetracyclin label (4 weeks) is red, calcein label (8 weeks) is green and xylenol orange label (12 weeks) is yellow. Bars indicate 1 mm.

Supplemental material

Figure 1 Defect bridging

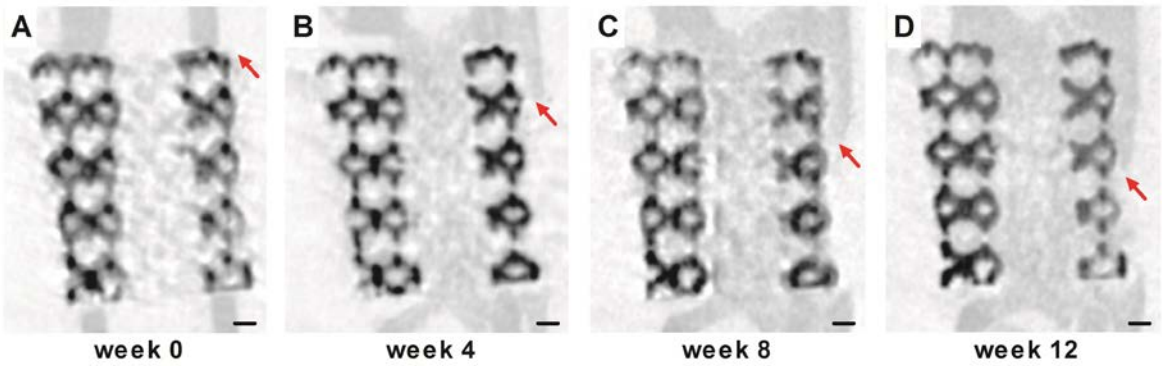

Figure 2 Resorption

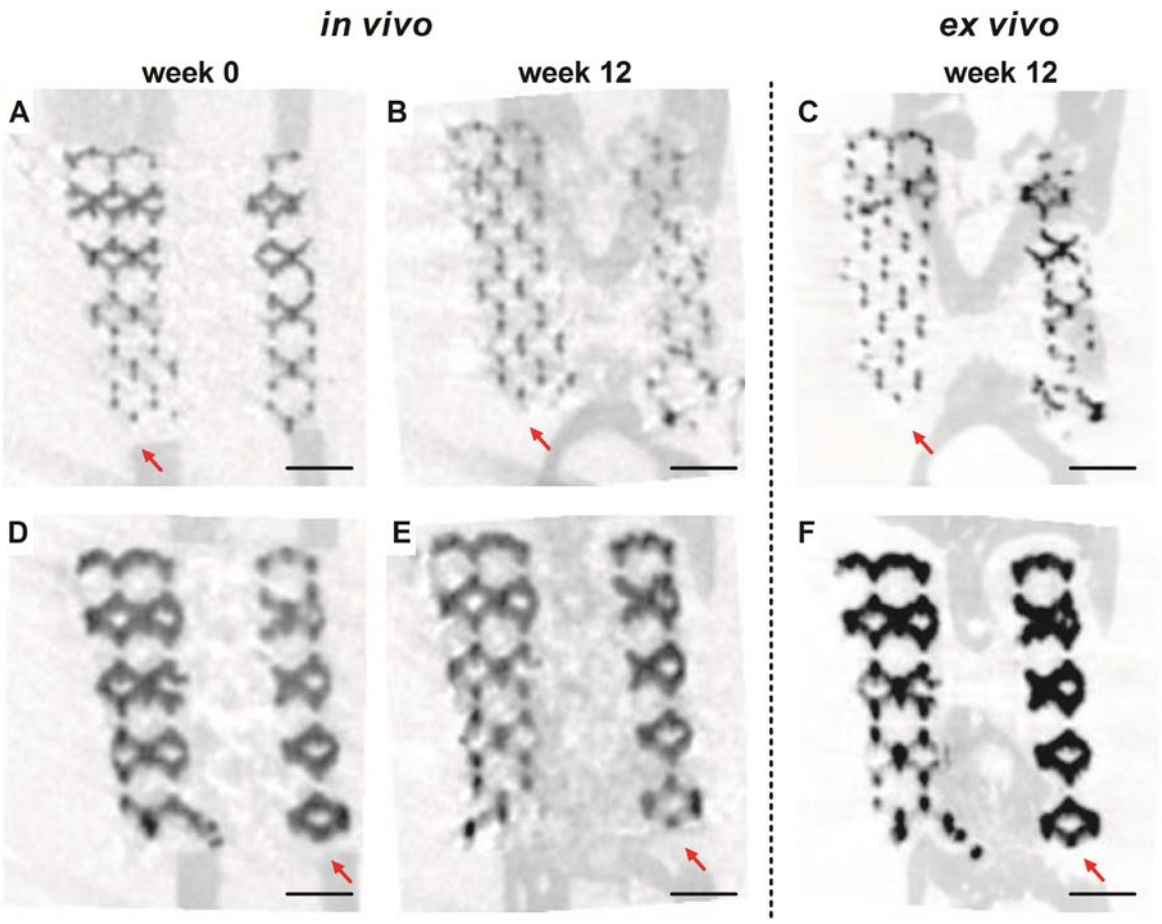

Figure 3 Empty defect

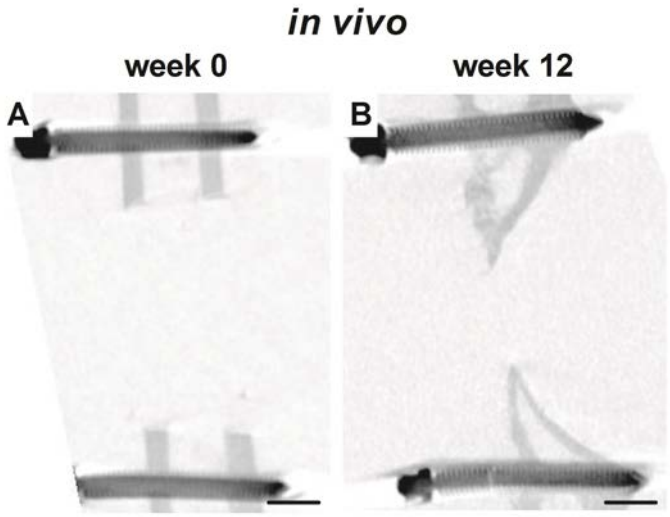

Figure 4 SEM image